UHASSELT
KNOWLEDGE IN ACTION

Maastricht University

Faculty of Medicine and Life Sciences
School for Life Sciences
Master of Biomedical Sciences

Master's thesis

Exploratory analysis of Epithelial rest of Malassez-Schwann cell-coupling in the periodontium via cholesterol transport

Kobe Wouters

Thesis presented in fulfillment of the requirements for the degree of Master of Biomedical Sciences, specialization Molecular Mechanisms in Health and Disease

SUPERVISOR :
Prof. dr. Ivo LAMBRICHTS

MENTOR :
dr. Florian HERMANS
dr. Karen LIBBERECHT

2025
2026

Transnational University Limburg is a unique collaboration of two universities in two countries: the University of Hasselt and Maastricht University.

UHASSELT
KNOWLEDGE IN ACTION

www.uhasselt.be
Universiteit Hasselt
Campus Hasselt:
Martelarenlaan 42 | 3500 Hasselt
Campus Diepenbeek:
Agoralaan Gebouw D | 3590 Diepenbeek

UHASSELT
KNOWLEDGE IN ACTION

Maastricht University

Faculty of Medicine and Life Sciences
School for Life Sciences
Master of Biomedical Sciences

Master's thesis

Exploratory analysis of Epithelial rest of Malassez-Schwann cell-coupling in the periodontium via cholesterol transport

Kobe Wouters

Thesis presented in fulfillment of the requirements for the degree of Master of Biomedical Sciences, specialization Molecular Mechanisms in Health and Disease

SUPERVISOR :

Prof. dr. Ivo LAMBRICHTS

MENTOR :

dr. Florian HERMANS

dr. Karen LIBBERECHT

Exploratory analysis of Epithelial rest of Malassez-Schwann cell-coupling in the periodontium via cholesterol transport*

Wouters K[1], Evens I[1], Ceyssens Z[1], Hermans F[1], Libberecht K[1,2,3] and Lambrichts I[1]

[1]Laboratory for Histology and Regeneration (HISTROGEN), Biomedical Research Institute (BIOMED), Universiteit Hasselt, Campus Diepenbeek, Agoralaan Gebouw C - B-3590 Diepenbeek
[2]VIB, Center for Brain & Disease Research, Laboratory of Neurobiology, Leuven, Belgium
[3]Laboratory for Functional Imaging & Research on Stem Cells (FIERCE), Biomedical Research Institute (BIOMED), Universiteit Hasselt, Campus Diepenbeek, Agoralaan Gebouw C - B-3590

*Running title: *ERM-Schwann Cell Cholesterol Crosstalk*

To whom correspondence should be addressed: Prof. dr. Ivo Lambrichts, Tel: +32 11 26 92 45; Email: ivo.lambrichts@uhasselt.be

Keywords: Periodontal ligament, Dental follicle, Immunohistochemistry, Cholesterol transport, epithelial cell rests of Malassez, Schwann cells

ABSTRACT

The periodontal ligament (PDL) is a mechanically demanding, highly innervated microenvironment. Schwann cells, the myelinating cells of the peripheral nervous system (PNS), require a substantial, continuous supply of cholesterol to maintain axonal myelination and support nerve function under these conditions, yet the local lipid transport mechanisms remain poorly understood. The epithelial cell rests of Malassez (ERM) are closely associated with periodontal nerves, suggesting they may serve as crucial supportive niche cells. This study investigates the spatial coupling between ERM and Schwann cells and evaluates the presence of cholesterol transport pathway components in the developing human dental follicle (DF) and mature PDL tissues. Singleplex and multiplex immunohistochemistry (IHC) and immunofluorescence (IF) were optimized and performed on human DF and PDL tissue sections. Samples were analyzed for cell-specific markers (TP63, CK14, MPZ, and β3-tubulin) and key components of the cholesterol transport pathway (APOE and LDLR), followed by the quantification of spatial distances. Tissue analysis revealed a close spatial proximity between ERM and Schwann cells/nerves, which was significantly shorter in the mature PDL than in the developing DF. Multiplex IHC confirmed that TP63-positive ERM cells express the core cholesterol transport components APOE and LDLR, with APOE also observed in adjacent Schwann cells and nervous structures. Ultimately, this histological evidence of spatial coupling and localized transport elements suggests that the ERM may function as a localized lipid-provisioning hub, supporting Schwann cell survival and maintaining periodontal innervation.

INTRODUCTION

Dental root development is an intricate process of epithelial-mesenchymal interactions initiated by Hertwig's epithelial root sheath (HERS). The disintegration of HERS into epithelial cell rests of Malassez (ERM) is a critical developmental event, as it permits mesenchymal cells from the dental follicle to interact with the newly formed root dentin. This interaction drives the differentiation of cells that form the periodontium, including the fibroblasts that synthesize the periodontal ligament (PDL). As a specialized connective tissue, the PDL anchors the tooth to the alveolar bone and transmits occlusal forces, a function supported by its highly vascularized and innervated nature (1, 2).

The PDL is intricately innervated, which is essential for the tissue's sensory capabilities. It comprises a diverse population of neuronal subtypes, including mechanosensory fibers responsible for proprioception, as well as nociceptive and thermosensitive fibers that detect pain and temperature (3). To maintain neural homeostasis and functionality, these neurons rely on a diverse cast of supportive niche cells (4).

Schwann cells, the main glial cells of the peripheral nervous system, are key supportive cells. They sustain nerve function through metabolic support and axonal myelination, facilitating fast signal conduction and neuronal survival (5). Schwann cells are derived from ventrally migrating neural crest cells, which sequentially differentiate into Schwann cell precursors and subsequently into immature Schwann cells upon interaction with developing embryonic nerve trunks. The maturation process involves radial sorting, a highly regulated mechanism driven by axonal-derived signals, such as neuregulin-1 type III, and axonal size. This process culminates in the differentiation of immature Schwann cells into either myelinating Schwann cells or non-myelinating Remak Schwann cells (5, 6).

Within the specific context of the PDL, Schwann cells continuously envelop larger axons, providing metabolic support and myelination necessary for rapid signal transduction. The myelination involves the concentric wrapping of the Schwann cell's plasma membrane around an axon, providing the structural stability and electrical insulation necessary for the rapid, saltatory conduction of nerve impulses (7-9). To achieve this structural feat, the myelin sheath has a high lipid content, comprising approximately 70%-85% of its dry mass. Consequently, Schwann cell function is intrinsically linked to lipid metabolism, as cholesterol availability, synthesis, and uptake are essential for proper myelination and axonal support (10, 11).

Previous research from the central and the peripheral nervous system outside the periodontium underscores the importance of these components, demonstrating that the local availability of cholesterol is a rate-limiting factor for both the initial establishment of innervation and the maintenance of nerve function (10, 12). Because Schwann cells must meet rapid metabolic demands, any disruption in this lipid supply chain compromises the integrity of the insulating sheath, leading to hypomyelination and sensory deficits (11, 13). While it is well established that Schwann cells carefully balance endogenous cholesterol synthesis with the uptake of exogenous lipoproteins to support proper myelination and nerve regeneration, how these essential lipid-dependent mechanisms operate within the unique, mechanically active microenvironment of the periodontium remains virtually unknown (13, 14). Unlike the relatively protected environment of the central nervous system, the PDL is a highly dynamic microenvironment subjected to constant occlusal forces, rapid tissue turnover, and the oral microbiome (14-16). For the local Schwann cell population, maintaining structural integrity and functional myelination under these mechanically demanding conditions likely requires continuous lipid remodeling and imposes unique metabolic constraints (7, 17). Consequently, it remains unclear how cholesterol is locally transported and utilized to constantly repair and support periodontal innervation within this stressed tissue. This uncertainty highlights a critical gap in our understanding of periodontal niche interactions.

Already in the 90s, our team identified the ERM as highly innervated by both myelinated and unmyelinated nerve fibers, placing it in close physical association with periodontal Schwann cells (18). Historically dismissed as functionless remnants of HERS, the ERM are now recognized as a dynamic cellular population that maintains a close association with local innervation and Schwann cells, suggesting they may function as an additional (18, 19), crucial support cell within the periodontal niche. Initially, HERS elongates apically, transmitting signals to the surrounding mesenchyme, which then triggers proliferation and differentiation into root odontoblasts, thereby driving root formation. As HERS extends apically, it progressively fragments coronally. This fragmentation stimulates the adjacent mesenchyme to differentiate into cementoblasts that deposit cementum against the root dentin. The remaining HERS epithelial cells disperse throughout the dental follicle, thereby establishing the ERM as a lace-like, fenestrated network within the PDL space (20). These cells retain a specific epithelial identity, as evidenced by markers such as Cytokeratin 14 (CK14) and p63, and are hypothesized to play a role in maintaining the width of the PDL space and preventing root resorption (21, 22). Independent of this stemness, ERM cells have also been shown to undergo Epithelial-Mesenchymal Transition in response to injury (23). Given their physical proximity to local nerve fibers, it is highly plausible that these epithelial cells interact dynamically with periodontal Schwann cells. However, studying their specific (metabolic) interactions is challenging with traditional cell cultures (24, 25).

To study cooperative interactions between ERM and Schwann cells in their native context, this research employs human dental follicle (DF) and periodontal ligament (PDL) tissues as primary models. Both tissue types are routinely obtained from donors undergoing extraction of impacted or orthodontically indicated third molars, making them a clinically accessible and translational resource. In unerupted teeth, the DF represents the developmental precursor to the PDL, a fibrous sac enveloping the crown that, upon tooth eruption, reorganizes into the mature periodontal ligament (26). Critically, both tissues harbor the native ERM population alongside their closely associated Schwann cell and neuronal elements, preserving the complex spatial organization and multicellular diversity that *in vitro* cell culture models inherently fail to recapitulate (27-29).

Preliminary data from our research group have provided a first insight into dynamic interactions between ERM and Schwann cells within the PDL during the establishment of periodontal innervation (data not shown), suggesting cell-cell communication between the cholesterol-mediated signaling pathways of both cell types, specifically via the Apolipoprotein A1 (APOA1)-ATP-binding cassette subfamily A (ABCA1) transporter axis (Figure 1).

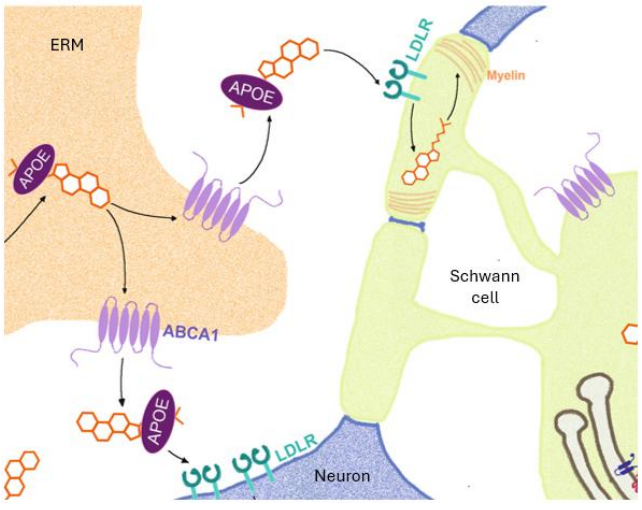

Figure 1– Cholesterol transport mechanism between the ERM and the SC suggested by the preliminary data. adjusted from (10)

By using sections of DF and PDL tissues for immunohistochemistry (IHC) and immunofluorescence (IF) analysis, it is possible to perform the *in situ* characterization of ERM–Schwann cell spatial relationships and the localization of cholesterol transport pathway components within intact periodontal tissue. By examining both the developing (DF) and mature (PDL) periodontal environment, this approach allows for a comparative assessment of whether key molecular interactions are conserved across different stages of tooth development, providing histological evidence for the presence of cholesterol transport components between ERM and Schwann cells (ERM → ABCA1 → APOE → LDLR → Schwann cell).

EXPERIMENTAL PROCEDURES

Collection of periodontal and dental pulp tissue – Ethical approval was obtained by the medical ethical committee of Ziekenhuis Oost-Limburg, Genk, Belgium (13/0104U). Human third molars and their dental follicle (DF) or PDL were collected with written informed consent from donors (15-20 years of age) undergoing routine tooth extraction for orthodontic or therapeutic reasons at Ziekenhuis Oost-Limburg. The DF, together with the PDL were fixed in 4% paraformaldehyde at 4°C for 24 h, and embedded in paraffin. These embedded tissues were sectioned (4 µm, unless differently mentioned) and used for immunohistochemistry (IHC) or immunofluorescence (IF) analysis (see further). Alternatively, The DF was dissociated into single cells as previously described (30, 31). Isolation of the tissue from the tooth was performed using a scalpel and washed successively in 70% ethanol, phosphate buffer saline (PBS), and DF collection medium (αMEM supplemented with 10% fetal calf serum (FCS), 0.5% Amphotericin B (Gibco, Thermo Fisher Scientific, Waltham, MA, USA), and 1% penicillin-streptomycin). Minced tissue (1 mm^2) was digested in PBS containing Collagenase VI (3 mg/ml, Thermo Fisher Scientific) and Dispase II (4 mg/ml, Sigma-Aldrich, Saint Louis, Mo, USA) for 2 hours at 37°C with periodic mechanical trituration. The suspension was treated with DNase I (0.2 mg/ml), filtered (40 µm), and centrifuged. Pelleted cells were resuspended in SFDM, mixed with growth factor-reduced, phenol red-free Matrigel (30:70), and plated as 20 µL droplets (20,000 cells).

Immunohistochemistry (IHC) – Formalin-fixed paraffin-embedded (FFPE) sections were baked at 58°C for 1 hour, deparaffinized in xylene,

and rehydrated through a graded ethanol series. Antigen retrieval was performed at 95°C in 10 mM citrate buffer with 0.05% Tween-20 (pH 6) for 20 minutes or in 1X TRIS-EDTA (pH 9, Proteintech) for 10 minutes. Endogenous peroxidase activity was blocked with 3% H_2O_2 for 10 minutes, followed by blocking in serum-free protein block (DAKO, Agilent Technologies, Santa Clara, CA, USA) for at least 1 hour at room temperature. Positive sections were incubated with primary antibodies (Supplementary table 1) overnight at 4°C, followed by secondary antibodies (Supplementary table 1) conjugated to either horseradish peroxidase or alkaline phosphatase for 30 minutes at room temperature. Negative controls were only incubated with a secondary antibody. Immunoreactivity was visualized using 3,3'-diaminobenzidine chromogen (DAB, Agilent Technologies), ImmPACT VIP (Vector Laboratories, Newark, CA, USA), ImmPACT Vector Red (Vector Laboratories) or BCIP/NBT (Vector Laboratories), either counterstained with 50% Gill's hematoxylin, blued in 0.02% ammonium water, or with Methyl Green counterstain (Vector Laboratories), dehydrated with a graded ethanol series and xylene, and mounted with EcoMount (Biocare Medical, Pacheco, CA, USA).

Multiplexed IHC staining – FFPE sections were baked at 58°C for 1 hour, deparaffinized in xylene, and rehydrated through a graded ethanol series. Antigen retrieval was performed in Citrate buffer (pH 6) for 20 minutes at 95°C. Endogenous peroxidase and phosphatase activity were blocked with BLOXALL Blocking solution (Vector Laboratories) for 10 minutes, followed by blocking in serum-free protein block (Agilent Technologies) for at least 1 hour at room temperature. Sections were incubated with the first primary antibody (Supplementary Table 1) overnight at 4°C. For multiplexed IHC, a single secondary antibody conjugated with horse radish peroxidase was incubated for 30 minutes at room temperature. Then, immunoreactivity was visualized using DAB (Agilent Technologies). Subsequently, a second protein-blocking step was performed with serum-free protein block (Agilent Technologies) for 1 hour, followed by overnight incubation with the next primary antibody at 4°C. Next, a corresponding secondary antibody conjugated to alkaline phosphatase was incubated, and the reaction was visualized with either ImmPACT Vector Red (Vector Laboratories) or BCIP/NBT (Vector Laboratories). This sequential process was repeated iteratively until all target markers were successfully stained. Finally, slides were counterstained, dehydrated, and mounted as described above.

The distance between the different cell types was measured using 3DHISTECH SlideViewer software, version 2.9.0. (3DHISTECH Kft., Budapest, Hungary). First, both cell populations were individually highlighted, and their perimeters were determined. Next, the distance between the perimeters was measured. This data was used for statistical analysis.

Immunofluorescence (IF)– For IF staining, FFPE slides were processed as described above. Following labeling with primary antibodies, slides were incubated with fluorescent probe-conjugated secondary antibodies (Alexa Fluor 488, 555, 594, 647, Invitrogen, Waltham, MA, USA) and Hoechst 33342 (Invitrogen) for 1 hour. Afterward, slides are mounted with ProLong Glass Antifade Mountant (Invitrogen).

Statistics – Statistical analysis was performed using the GraphPad Prism, version 10.6.1 (GraphPad Software, San Diego, CA, USA). Data normality was assessed using the Shapiro-Wilk test. For normally distributed data, comparisons between two groups were performed using a unpaired Student's t-test. For non-normally distributed data, comparisons between two groups were performed using the Mann-Whitney test.

RESULTS

Singleplex and multiplex IHC on multiple markers paved the way for optimal multiplex IHC combinations – To identify the optimal marker combination and visualization color scheme, multiple optimization stainings were performed. First, singleplex IHC assays for CK14, TP63, GFAP, and MBP were evaluated to determine the most reliable markers for ERM and Schwann cells, respectively (Supplementary Figure 1). While CK14 showed promise, TP63 was ultimately selected due to its distinct nuclear localization as a transcription factor. This strict nuclear targeting minimizes potential spatial overlap with other cytoplasmic or membrane-bound ERM markers, such as APOE or LDLR. Regarding the Schwann cell markers, both GFAP and MBP demonstrated negligible differences in immunoreactivity between

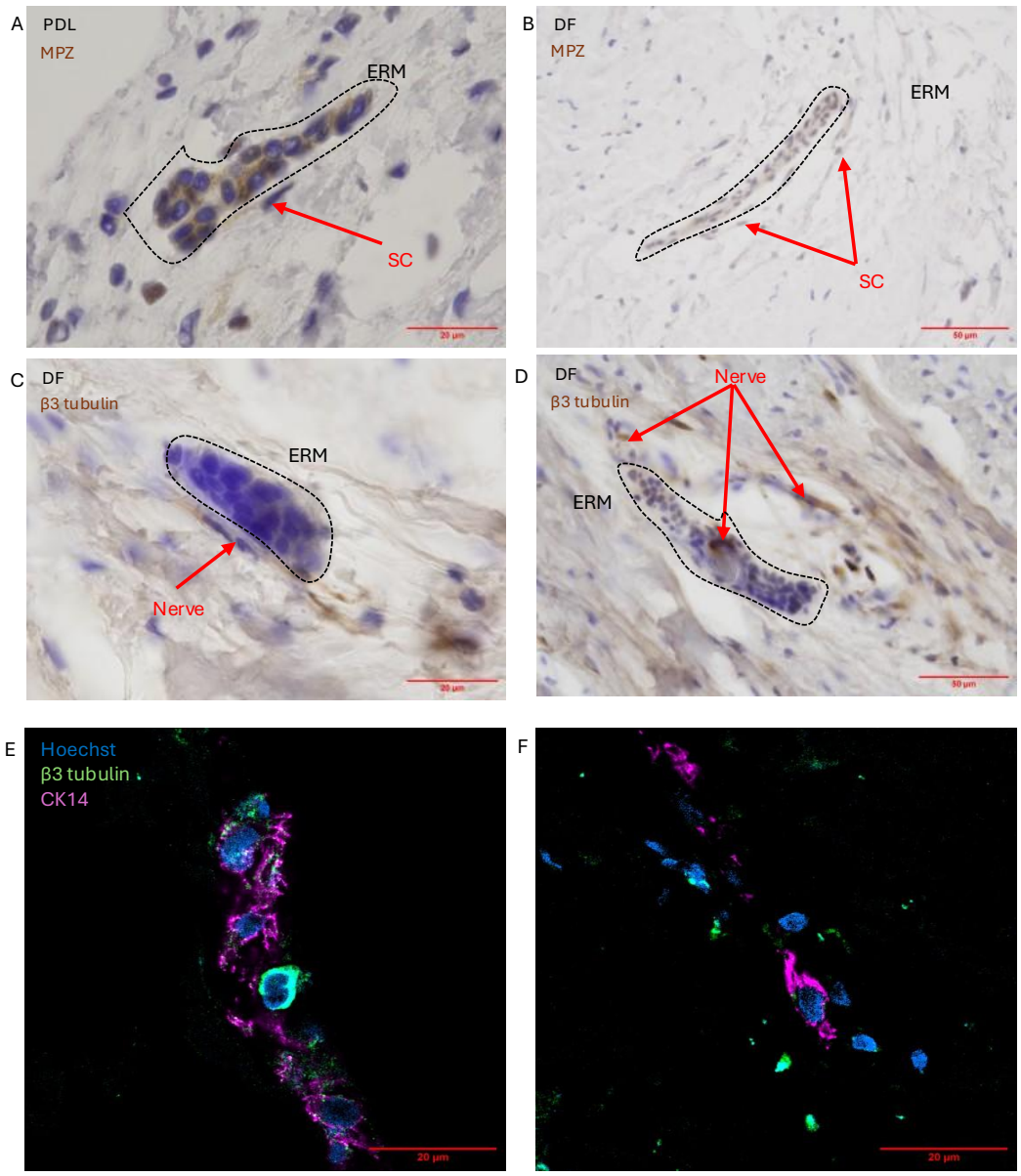

Figure 2 – Immunohistochemical and immunofluorescent staining of PDL and DF tissue. IHC-DAB micrographs of thin PDL (A) and DF sections (4 µm) (B) stained for MPZ (brown). (C, D) IHC-DAB micrographs of thick DF sections (20 µm) stained for β3-tubulin (Brown). (E, F) Immunofluorescence staining of DF sections for β3-tubulin (green) and CK14 (magenta), with a Hoechst Nuclear staining (Blue).

positive samples and negative controls. Consequently, based on these evaluation rounds and prior staining success, myelin protein zero (MPZ) was selected as the definitive Schwann cell marker.

Subsequently, the integration of MPZ and the cholesterol transport components (APOE or LDLR) with the nuclear ERM marker was optimized using sequential multiplex IHC (Supplementary Figure 2). This protocol enabled the co-visualization of MPZ, APOE, or LDLR with TP63 in a single tissue section. Minor TP63 immunoreactivity occasionally observed in the negative controls during these test runs was attributed to accidental cross-contamination or to primary antibody spillage during parallel incubation. This artifact was strictly

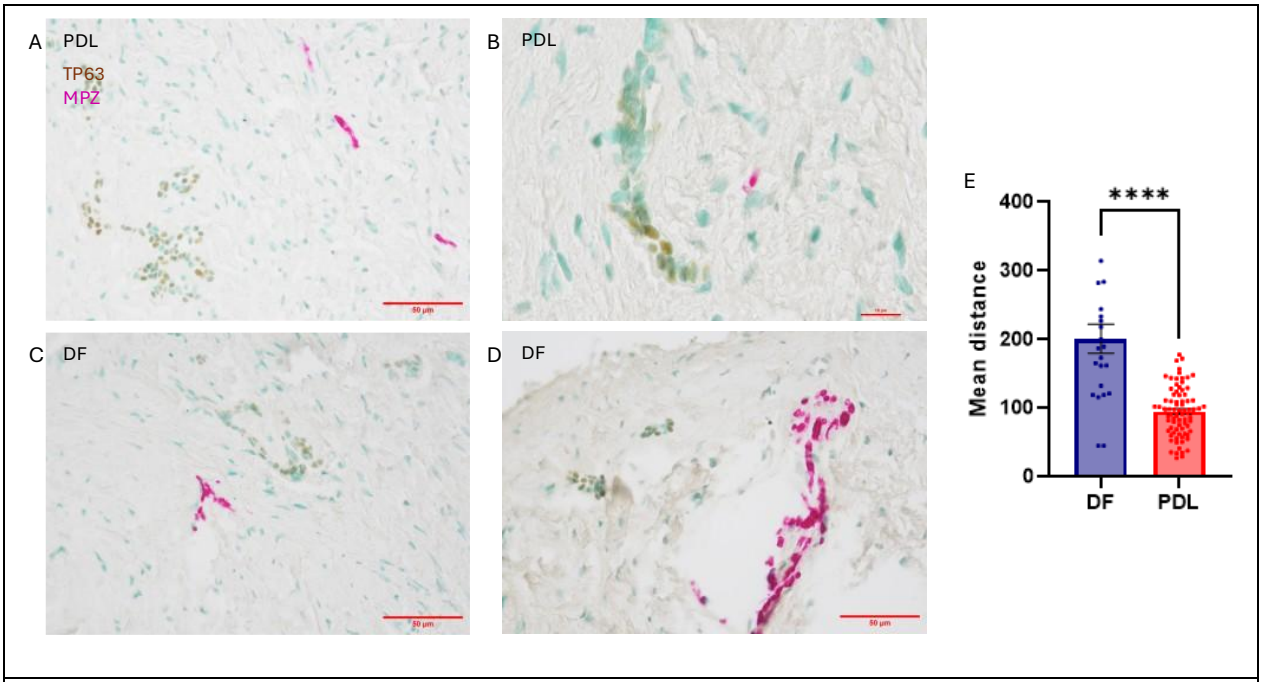

Figure 3 – Multiplex immunohistochemical labeling and spatial analysis of TP63 and MPZ. (A, B) Multiplex IHC micrographs of PDL sections and (C, D) DF sections. TP63 immunoreactivity is visualized in brown, while MPZ expression is visualized in pink. Nuclei are counterstained with methyl green. (E) Quantitative analysis representing the mean distance between TP63-positive and MPZ-positive cells. ****p<0,0001. Data is shown as Mean ± SEM. Statistical analysis was performed with the Mann-Whitney test. N=7 with 3 technical repeats

confined to the concurrent optimization rounds for APOE and LDLR and was subsequently resolved. Taken together, these optimization steps established a robust staining panel, enabling the simultaneous detection of ERM, Schwann cells/nerves, and the cholesterol transport mechanism.

Tissue analysis shows a close association between ERM and Schwann cells/nerve tissue – To evaluate the close proximity between ERM and SCs *in situ*, single and multiplex IF/IHC were performed on PDL and DF samples from different donors (Figure 2). First, expression of markers expressed by both ERM (MPZ), nervous tissue (β3-tubulin), or SC (MPZ, β3-tubulin) (Figure 2A-D). IF co-labeling of CK14 (expressed by ERM) and axonally-localized β3-tubulin (Figure 2E-F) confirmed the close association observed between ERM and peripheral innervation. Additionally, DF and PDL tissues were labeled with MPZ (myelinating Schwann cells/nervous tissue) and TP63, a transcription factor expressed in ERM nuclei (Figure 3A-D). Quantification of ERM-Schwann distance showed a significantly shorter distance in the PDL (94,51±3,979 µm) compared to the DF (200,8±21,44 µm) (Figure 3E).

Cholesterol pathway components are present in both PDL and DF tissue – Based on our preliminary hypotheses, we performed singleplex IHC analysis to verify if the proposed cholesterol transport pathway is present in PDL and DF tissues (Figure 4). It demonstrates the presence of the APOE transporter in both PDL and DF tissues, specifically localized within the ERM and Schwann cells/nerves. Additionally, LDLR was identified within the ERM of both tissue types, but not in Schwann cells/nerves.

Multiplex IHC confirms ERM-Schwann cell association and transport components– To simultaneously confirm the identity of the ERM and the localization of the cholesterol transport components within the same tissue section, multiplexed IHC was performed on both DF and PDL tissue. TP63 (ERM) was labeled in combination with either APOE or LDLR. Co-staining of TP63 and APOE on DF tissue (Figure 5A) and PDL tissue (Figure 5B) confirmed the presence of APOE within TP63-positive ERM cells, confirming the single-marker IHC findings

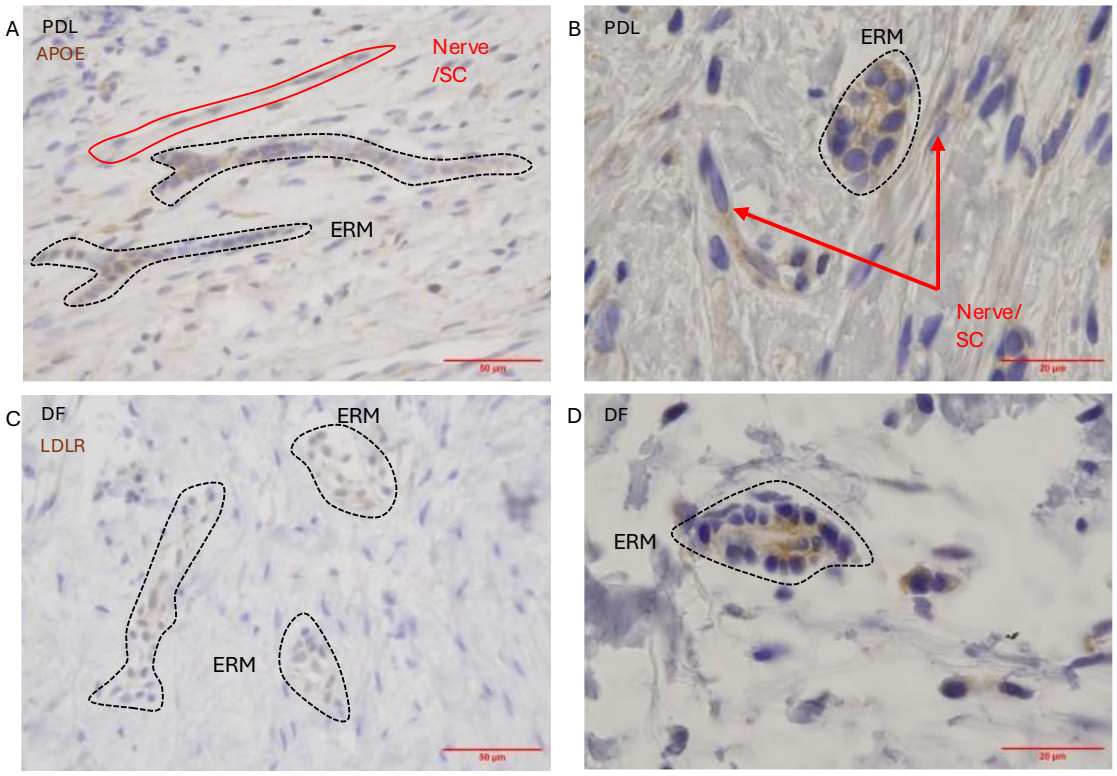

Figure 4 – Immunohistochemical labeling of APOE and LDLR in periodontal ligament and dental follicle tissues. (A, B) IHC-DAB micrographs of PDL sections stained for APOE. (C, D) IHC-DAB micrographs of DF sections stained for LDLR.

and localizing this cholesterol transporter within the ERM population. Similarly, multiplexed staining of TP63 and LDLR on DF (Figure 5C) and PDL tissue (Figure 5D) confirmed the presence of LDLR within TP63-positive ERM cells, further supporting the hypothesis that ERM cells are equipped for cholesterol transport.

As a final confirmation of the presence of transport components and the close association between ERM and Schwann cells/nerves, an additional multiplex IHC was performed for MPZ (Schwann cells/nerves), APOE (cholesterol transport), and TP63 (ERM) (Figure 6). Here, overlap in coloring was observed for APOE and TP63, and for APOE and MPZ (Figure 6A-D), while an additional distance analysis showed that the distance between ERM and Schwann cells/nerves was shorter in PDL (91,16±5,537 µm) than in DF (196,7±19,29 µm) (Figure 6E).

DISCUSSION

The PDL is a highly dynamic and mechanically stressed microenvironment that sustains cyclic occlusal forces during mastication (32). Within this mechanically demanding niche, robust innervation is required to provide essential sensory feedback and maintain tissue homeostasis (33). Our preliminary data provided the first evidence supporting possible cholesterol crosstalk between the ERM and local Schwann cells within this niche. The histological analysis of PDL and DF tissues demonstrated a close spatial association between ERM and Schwann cells, which becomes significantly closer as the tissue matures from DF to mature PDL. Furthermore, IHC confirmed that ERM express core cholesterol transport components, namely APOE and LDLR. Because myelinating Schwann cells in the PNS have massive, continuous lipid requirements, particularly for cholesterol, to assemble and maintain axonal myelination, our data suggest that ERM can act as a localized lipid-provisioning hub to help Schwann cells survive the constant mechanical stress of the periodontium (34, 35).

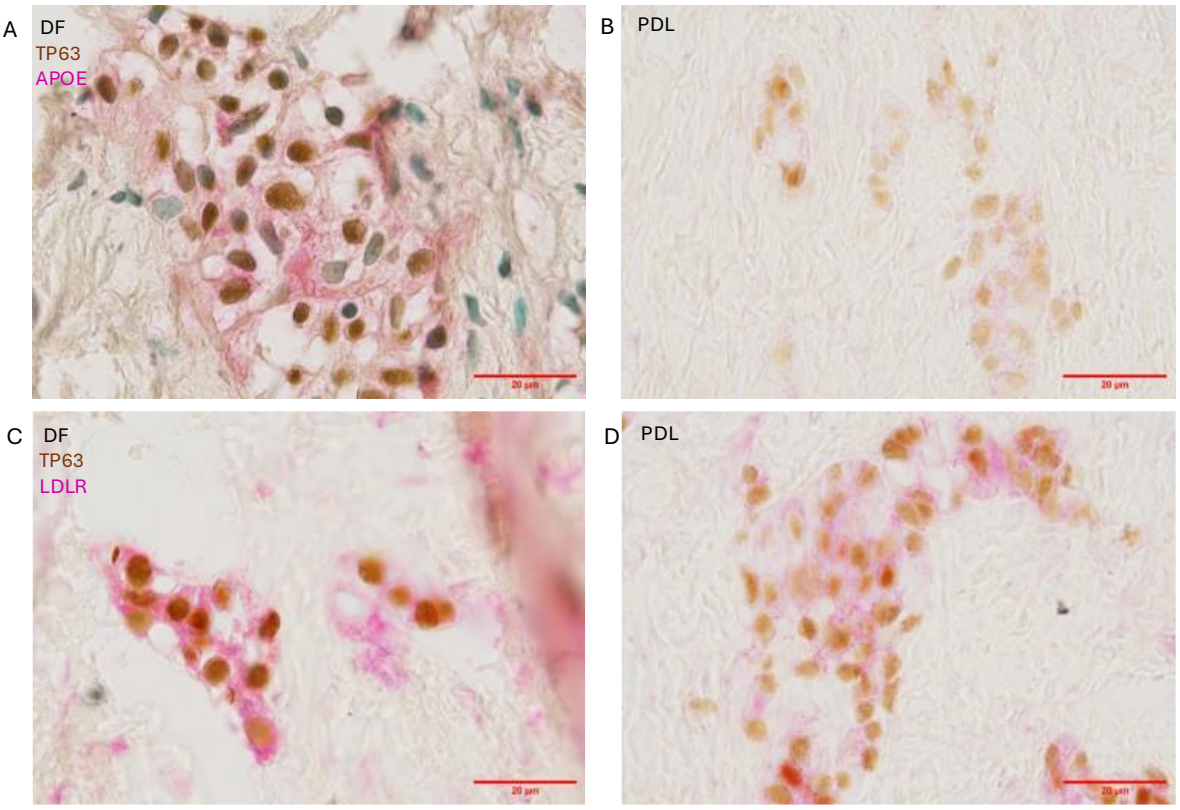

Figure 5 – Multiplex immunohistochemical labeling of APOE, LDLR, and TP63 in DF and PDL tissues. (A) Multiplex IHC micrographs of DF sections and (B) PDL sections stained for Apolipoprotein E (APOE, pink) and Tumor Protein 63 (TP63, brown). (C) Multiplex IHC micrographs of DF sections and (D) PDL sections stained for LDLR (pink) and TP63 (brown).

Our spatial analysis demonstrating a close physical association between ERM and Schwann cells aligns with previous immunohistochemical investigations of the periodontal niche. Earlier mappings of the spatial interrelation between the root surface and the periodontal membrane established that innervation is localized in close proximity to the epithelial layer of Malassez, which acts as a structural border within the fiber morphology (36). The multiplex IHC performed for MPZ and TP63, and MPZ, APOE, and TP63 confirmed this observation.

The concept that ERM and local nerve structures engage in vital, bidirectional crosstalk is supported by the literature. Yamashiro et al. (2000) demonstrated that ERM selectively expresses TrkA, the high-affinity receptor for Nerve Growth Factor (NGF). Additionally, they demonstrated that sensory denervation of the tooth resulted in a marked decrease in the size and distribution of ERM clusters, suggesting that neural innervation is required to maintain the epithelial rests in the PDL (19). While their work established that nerves regulate the survival of the ERM, our findings suggest the inverse may also be true: the ERM may sustain the local peripheral nervous network. However, this needs further research for confirmation.

The ERM has recently been classified as a dynamic, stem cell-like population capable of secreting a wide array of paracrine factors, including cytokines, chemokines, and growth factors, to maintain periodontal homeostasis (22). However, this is not widely recognized, which is why the specific role of ERM in lipid metabolism and cholesterol transport has remained entirely unexplored in healthy periodontal tissue. By demonstrating that ERM express components of the cholesterol transport pathway (APOE and LDLR), our data introduce a novel perspective. We propose that the ERM secretory function extends beyond protein-based growth factors to include critical lipid

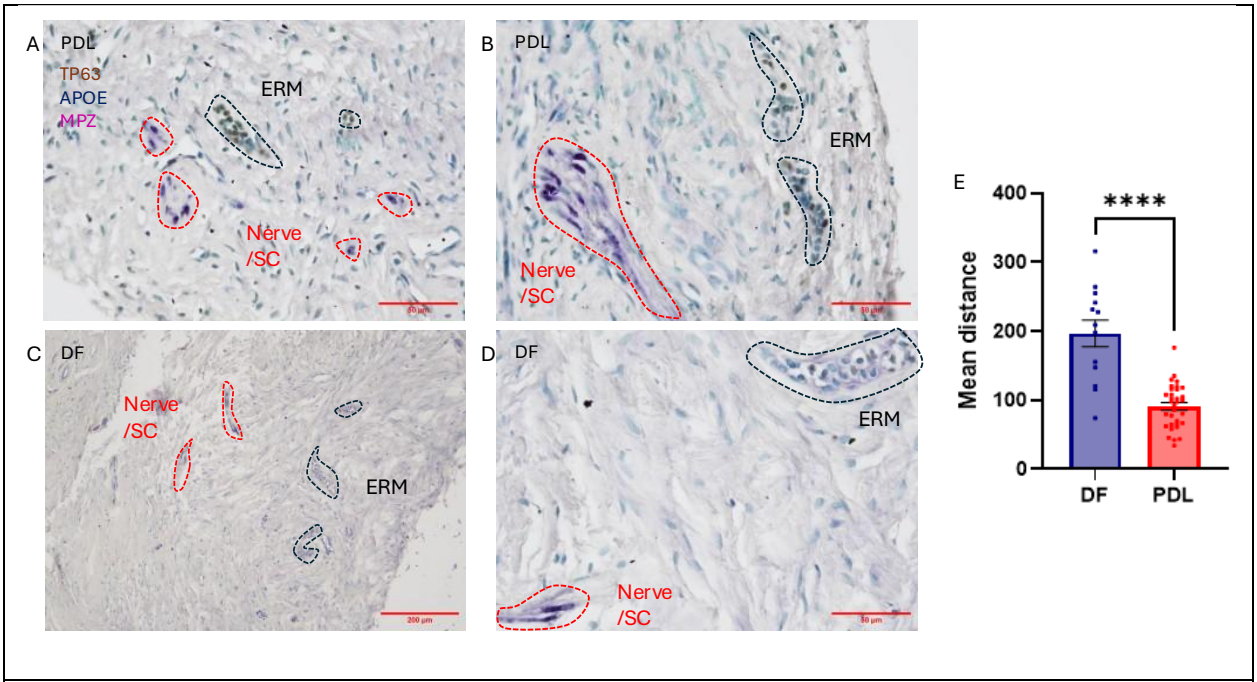

Figure 6 – Multiplex immunohistochemical labeling of MPZ, APOE, and TP63 in DF and PDL tissues. (A-B) Multiplex IHC micrographs of PDL sections stained for MPZ (pink), APOE (blue), and TP63 (brown). (C-D) Multiplex IHC micrographs of DF sections stained for MPZ (pink), APOE (blue), and TP63 (brown). (E) Quantitative analysis representing the mean distance between TP63-positive and MPZ-positive cells. ***p<0,001. Data is shown as Mean ± SEM. Statistical analysis was performed with the Mann-Whitney test. N=10 with 2 technical repeats

provisioning. Because Schwann cells in the mechanically stressed periodontal ligament require immense amounts of cholesterol for myelin maintenance and membrane stability, the ERM can act as a localized, essential metabolic hub. By demonstrating a metabolic relationship via cholesterol transport, our findings provide a functional explanation for the morphological proximity documented by Bille et al. (2009). Furthermore, this lipid-based support complements the neurotrophic signaling described by Yamashiro et al. (2000), thereby offering a more comprehensive model of the periodontal neuro-epithelial axis.

However, while these static immunohistochemical observations confirm the presence and localization of this transport machinery, they have considered only myelinated nervous tissue and myelinating Schwann cells. Additionally, they also cannot capture the dynamic cell-to-cell metabolic crosstalk (37). As highlighted in previous studies, studying complex epithelial-mesenchymal or epithelial-neural interactions is inherently challenging using traditional 2D monolayer cell cultures, which fail to preserve spatial organization and native cellular phenotypes.

To bridge the gap between our static *in situ* immunohistochemical observations and dynamic functional validation, transitioning from traditional 2D monolayers to advanced 3D models is essential. While flat cell cultures fail to capture native tissue complexity, ERM-derived tissue organoids (ERM-TO) faithfully preserve the architectural integrity, epithelial identity, and stem cell characteristics of the native ERM (24, 30, 31). However, to fully unravel the completely unexplored metabolic cooperation between the ERM and Schwann cells during periodontal innervation, an 'assembloid' approach represents the next critical frontier. By combining ERM-TOs with specific Schwann cell lineages into a spatially organized 3D structure, future research can accurately recapitulate the cellular diversity and physical architecture of the periodontal niche (37-40). Ultimately, this platform will provide the dynamic environment needed to systematically dissect and validate the functional neuroepithelial crosstalk proposed in this study.

To systematically investigate these interactions, our research team has developed a

novel 3D periodontal assembloid model by co-culturing human ERM-derived organoids with dental pulp stem cell-derived Schwann cells (DPSC-SCs) (41, 42). This approach could create a highly controlled, physiologically relevant microenvironment where epithelial and glial components can physically interact. By leveraging these assembloids, it will be possible to move past purely observational histology and functionally interrogate the predicted cholesterol transport pathways, directly evaluating their real-time influence on Schwann cell function. Ultimately, uncovering these mechanisms will provide a fundamental, mechanistic understanding of the neural niche within the PDL and DF, potentially revealing new therapeutic targets to maintain or regenerate periodontal sensory function.

CONCLUSION

This exploratory study provides novel histological evidence suggesting metabolic interplay between the ERM and local Schwann cells within the periodontium's dynamic microenvironment. Our findings confirm a close spatial association between these two cell populations, which becomes significantly more pronounced as the tissue matures from the DF to the PDL. Furthermore, multiplexed immunohistochemical analysis demonstrates that the ERM expresses core components of the cholesterol transport pathway, specifically APOE and the LDLR.

Collectively, these results suggest a paradigm shift in our understanding of the ERM, extending its recognized secretory capabilities to include critical lipid provisioning. By supplying essential cholesterol, the ERM may function as a localized metabolic hub. This enables Schwann cells to meet the massive lipid demands required to maintain structural integrity and axonal myelination under the constant mechanical stress of mastication. Ultimately, this bidirectional ERM-neural crosstalk may prove essential to sustain the robust (sensory) innervation required for periodontal homeostasis. Further functional studies are warranted to fully elucidate the dynamics of this cholesterol-mediated transport mechanism and its potential therapeutic implications for periodontal regeneration and neural repair.

REFERENCES

1. Li J, Parada C, Chai Y. Cellular and molecular mechanisms of tooth root development. Development. 2017;144(3):374–84.
2. Duan Y, Liang Y, Yang F, Ma Y. Neural Regulations in Tooth Development and Tooth-Periodontium Complex Homeostasis: A Literature Review. Int J Mol Sci. 2022;23(22).
3. Wang S, Ko CC, Chung MK. Nociceptor mechanisms underlying pain and bone remodeling via orthodontic forces: toward no pain, big gain. Front Pain Res (Lausanne). 2024;5:1365194.
4. Kaukua N, Shahidi MK, Konstantinidou C, Dyachuk V, Kaucka M, Furlan A, et al. Glial origin of mesenchymal stem cells in a tooth model system. Nature. 2014;513(7519):551–4.
5. Jessen KR, Mirsky R, Lloyd AC. Schwann Cells: Development and Role in Nerve Repair. Cold Spring Harb Perspect Biol. 2015;7(7):a020487.
6. Monk KR, Feltri ML, Taveggia C. New insights on Schwann cell development. Glia. 2015;63(8):1376–93.
7. Poitelon Y, Kopec AM, Belin S. Myelin Fat Facts: An Overview of Lipids and Fatty Acid Metabolism. Cells. 2020;9(4).
8. Saher G, Quintes S, Mobius W, Wehr MC, Kramer-Albers EM, Brugger B, et al. Cholesterol regulates the endoplasmic reticulum exit of the major membrane protein P0 required for peripheral myelin compaction. J Neurosci. 2009;29(19):6094–104.
9. Montani L, Pereira JA, Norrmen C, Pohl HBF, Tinelli E, Trotzmuller M, et al. De novo fatty acid synthesis by Schwann cells is essential for peripheral nervous system myelination. J Cell Biol. 2018;217(4):1353–68.
10. Ho WY, Hartmann H, Ling SC. Central nervous system cholesterol metabolism in health and disease. IUBMB Life. 2022;74(8):826–41.
11. Orth M, Bellosta S. Cholesterol: its regulation and role in central nervous system disorders. Cholesterol. 2012;2012:292598.
12. Saher G, Brugger B, Lappe-Siefke C, Mobius W, Tozawa R, Wehr MC, et al. High cholesterol level is essential for myelin membrane growth. Nat Neurosci. 2005;8(4):468–75.
13. Saher G, Quintes S, Nave KA. Cholesterol: a novel regulatory role in myelin formation. Neuroscientist. 2011;17(1):79–93.
14. Zhang X, Yuan X, Xu Q, Arioka M, Van Brunt LA, Shi Y, et al. Molecular Basis for

Periodontal Ligament Adaptation to In Vivo Loading. J Dent Res. 2019;98(3):331–8.
15. McCormack SW, Witzel U, Watson PJ, Fagan MJ, Groning F. The biomechanical function of periodontal ligament fibres in orthodontic tooth movement. PLoS One. 2014;9(7):e102387.
16. Easter QT, Fernandes Matuck B, Beldorati Stark G, Worth CL, Predeus AV, Fremin B, et al. Single-cell and spatially resolved interactomics of tooth-associated keratinocytes in periodontitis. Nat Commun. 2024;15(1):5016.
17. Belin S, Zuloaga KL, Poitelon Y. Influence of Mechanical Stimuli on Schwann Cell Biology. Front Cell Neurosci. 2017;11:347.
18. Lambrichts I, Creemers J, Van Steenberghe D. Periodontal neural endings intimately relate to epithelial rests of Malassez in humans. A light and electron microscope study. J Anat. 1993;182 (Pt 2)(Pt 2):153–62.
19. Yamashiro T, Fujiyama K, Fukunaga T, Wang Y, Takano-Yamamoto T. Epithelial rests of Malassez express immunoreactivity of TrkA and its distribution is regulated by sensory nerve innervation. J Histochem Cytochem. 2000;48(7):979–84.
20. Hermans F, Hemeryck L, Lambrichts I, Bronckaers A, Vankelecom H. Intertwined Signaling Pathways Governing Tooth Development: A Give-and-Take Between Canonical Wnt and Shh. Front Cell Dev Biol. 2021;9:758203.
21. Xiong J, Mrozik K, Gronthos S, Bartold PM. Epithelial cell rests of Malassez contain unique stem cell populations capable of undergoing epithelial-mesenchymal transition. Stem Cells Dev. 2012;21(11):2012–25.
22. Xiong J, Gronthos S, Bartold PM. Role of the epithelial cell rests of Malassez in the development, maintenance and regeneration of periodontal ligament tissues. Periodontol 2000. 2013;63(1):217–33.
23. Liu B, Hermans F, Aellos F, Dworan J, Chang E, Clavelier A, et al. Injury-Activated ERMs Undergo EMT and May Contribute to Periodontal Repair. J Dent Res. 2025:220345251397858.
24. Hermans F, Hemeryck L, Bueds C, Torres Pereiro M, Hasevoets S, Kobayashi H, et al. Organoids from mouse molar and incisor as new tools to study tooth-specific biology and development. Stem Cell Reports. 2023;18(5):1166–81.
25. Clevers H. Modeling Development and Disease with Organoids. Cell. 2016;165(7):1586–97.
26. Bastos VC, Gomez RS, Gomes CC. Revisiting the human dental follicle: From tooth development to its association with unerupted or impacted teeth and pathological changes. Dev Dyn. 2022;251(3):408–23.
27. Keinan D, Cohen RE. The significance of epithelial rests of Malassez in the periodontal ligament. J Endod. 2013;39(5):582–7.
28. Atsumi Y, Imai T, Matsumoto K, Sakuda M, Maeda T, Kurisu K, et al. Effects of different types of injury to the inferior alveolar nerve on the behavior of Schwann cells during the regeneration of periodontal nerve fibers of rat incisor. Arch Histol Cytol. 2000;63(1):43–54.
29. Luukko K, Moe K, Sijaona A, Furmanek T, Hals Kvinnsland I, Midtbo M, et al. Secondary induction and the development of tooth nerve supply. Ann Anat. 2008;190(2):178–87.
30. Hemeryck L, Lambrichts I, Bronckaers A, Vankelecom H. Establishing Organoids from Human Tooth as a Powerful Tool Toward Mechanistic Research and Regenerative Therapy. J Vis Exp. 2022(182).
31. Hemeryck L, Hermans F, Chappell J, Kobayashi H, Lambrechts D, Lambrichts I, et al. Organoids from human tooth showing epithelial stemness phenotype and differentiation potential. Cell Mol Life Sci. 2022;79(3):153.
32. Lin JD, Jang AT, Kurylo MP, Hurng J, Yang F, Yang L, et al. Periodontal ligament entheses and their adaptive role in the context of dentoalveolar joint function. Dent Mater. 2017;33(6):650–66.
33. Militi A, Cutroneo G, Favaloro A, Matarese G, Di Mauro D, Lauritano F, et al. An immunofluorescence study on VEGF and extracellular matrix proteins in human periodontal ligament during tooth movement. Heliyon. 2019;5(10):e02572.
34. Salzer JL. Schwann cell myelination. Cold Spring Harb Perspect Biol. 2015;7(8):a020529.
35. Barnes-Velez JA, Aksoy Yasar FB, Hu J. Myelin lipid metabolism and its role in myelination and myelin maintenance. Innovation (Camb). 2023;4(1):100360.
36. Bille ML, Nolting D, Kjaer I. Immunohistochemical studies of the periodontal

membrane in primary teeth. Acta Odontol Scand. 2009;67(6):382–7.
37. Jensen C, Teng Y. Is It Time to Start Transitioning From 2D to 3D Cell Culture? Front Mol Biosci. 2020;7:33.
38. Rockel AF, Wagner N, Spenger P, Ergun S, Worsdorfer P. Neuro-mesodermal assembloids recapitulate aspects of peripheral nervous system development in vitro. Stem Cell Reports. 2023;18(5):1155–65.
39. Onesto MM, Kim JI, Pasca SP. Assembloid models of cell-cell interaction to study tissue and disease biology. Cell Stem Cell. 2024;31(11):1563–73.
40. Liu F, Xiao J, Chen LH, Pan YY, Tian JZ, Zhang ZR, et al. Self-assembly of differentiated dental pulp stem cells facilitates spheroid human dental organoid formation and prevascularization. World J Stem Cells. 2024;16(3):287–304.
41. Martens W, Sanen K, Georgiou M, Struys T, Bronckaers A, Ameloot M, et al. Human dental pulp stem cells can differentiate into Schwann cells and promote and guide neurite outgrowth in an aligned tissue-engineered collagen construct in vitro. FASEB J. 2014;28(4):1634–43.
42. Libberecht K, Dirkx N, Vangansewinkel T, Vandendries W, Lambrichts I, Wolfs E. The Influence of Lysosomal Stress on Dental Pulp Stem Cell-Derived Schwann Cells. Biomolecules. 2024;14(4).
This document was supported by GenAI

Acknowledgments – dr. Florian Hermans, dr. Karen Libberecht and Prof. dr. Ivo Lambrichts are thanked for their guidance and assistance during the internship. Inya Evens and Ziggy Ceyssens are thanked for their aid during the experiments and data analysis. Prof. dr. Ivo Lambrichts is thanked for the opportunity to perform the internship at the Laboratory for Histology and Regeneration (HISTROGEN).

Author contributions – K.W. designed concepts and experiments, performed the experiments and data analysis, interpreted results, and wrote the manuscript. I.E. and Z.C. contributed in performing the experiments and data analysis. F.H co-designed the concepts and experiments, performed experiments, analyzed data, interpreted results, and contributed to writing, editing, and reviewing the manuscript. K.L. co-designed the concepts and experiments and contributed to data analysis, interpretation, writing, editing, and manuscript review. I.L. supervised the project and co-interpreted the results.

Supplementary Table 1 – Markers and Antibodies used in the various stainings

Name	Type of antibody	Antibody specs
APOE	Primary	Anti-APOE polyclonal rabbit IgG (HPA0065539, Atlas Antibodies) 1/500 dilution
CK14	Primary	Anti-CK14 monoclonal mouse IgG (MA5-11599, Invitrogen) 1/1000 dilution
LDLR	Primary	Anti-LDLR polyclonal rabbit IgG (HPA009647, Atlas Antibodies) 1/50 dilution
MBP	Primary	Anti-MBP rat monoclonal IgG (MAB386, Merck KGaA) 1/200 dilution
MPZ	Primary	Anti-MPZ polyclonal rabbit IgG (ab31851, Abcam Limited) 1/250 dilution
β3-tubulin	Primary	Anti-β3-tubulin mouse monoclonal IgG (T8578, Merck KGaA) 1/400 dilution
TP63	Primary	Anti-p63 Monoclonal rabbit IgG (ab124762, Abcam Limited) 1/3000 dilution
GFAP	Primary	Anti-EGR2 monoclonal rabbit IgG (ab245288, Abcam Limited) 1/400 dilution
Alexa Fluor 488	Secondary (Fluorescence)	Alexa fluor 488 IgG (H+L), anti-rat (2534074, Invitrogen) 1/1000 dilution
Alexa Fluor 555	Secondary (Fluorescence)	Alexa fluor 555 IgG (H+L), anti-rabbit (2873783, Invitrogen) 1/1000 dilution
Alexa Fluor 647	Secondary (Fluorescence)	Alexa fluor 647 IgG (H+L), anti-mouse (2674387, Invitrogen) 1/1000 dilution
Anti-mouse HRP	Secondary (Histochemistry)	Goat anti-mouse Polyclonal IgG (P0447, Aligent DAKO) 1/100 dilution
Anti-rabbit HRP	Secondary (Histochemistry)	Goat anti-rabbit Polyclonal IgG (P0448, Aligent DAKO) 1/100 dilution
Anti-Rabbit ALP	Secondary (Histochemistry)	ImmPRESS-AP Horse anti-rabbit IgG, ALP (MP-5401-15, Vector Laboratories)

APOE: Apolipoprotein E, CK14: Cytokeratin 14, LDLR: Low-Density Lipoprotein Receptor, MBP: Myelin Base Protein, MPZ: Myelin Protein Zero, TP63: Tumor Protein 63, GFAP: Glial fibrillary acidic protein, HRP: Horseradish Peroxidase, ALP: Alkaline Phosphatase

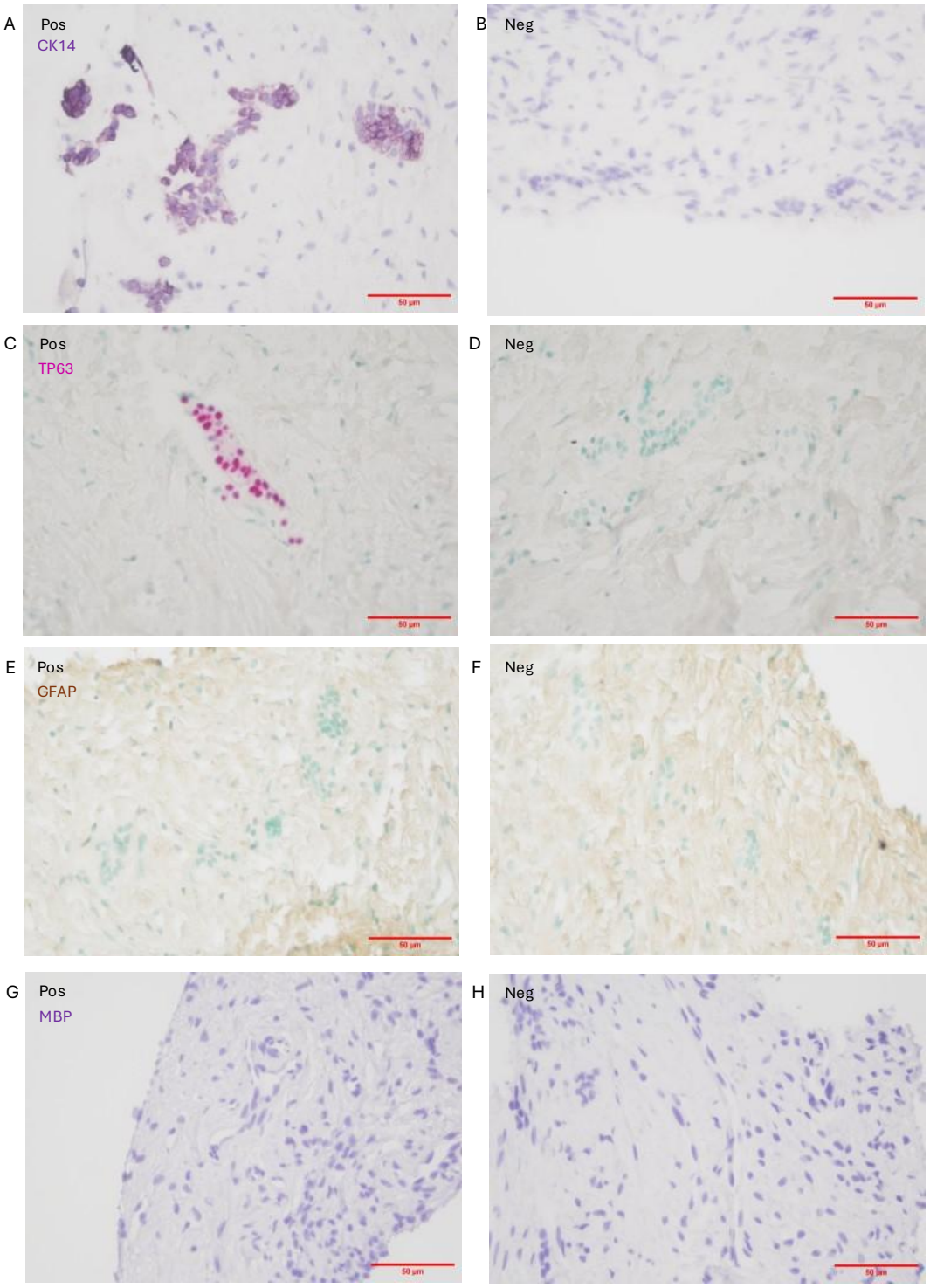

Supplementary Figure 1 – Optimization of ERM and Schwann cell marker DF and PDL tissues. Positive (A) and negative (B) IHC micrographs of PDL sections stained for CK14 (purple). Positive (C) and negative (D) IHC micrographs of DF sections stained for TP63 (pink). Positive (E) and negative (F) IHC micrographs of PDL sections stained for GFAP (brown). Positive (G) and negative (H) IHC micrographs of PDL sections stained for MBP (purple).

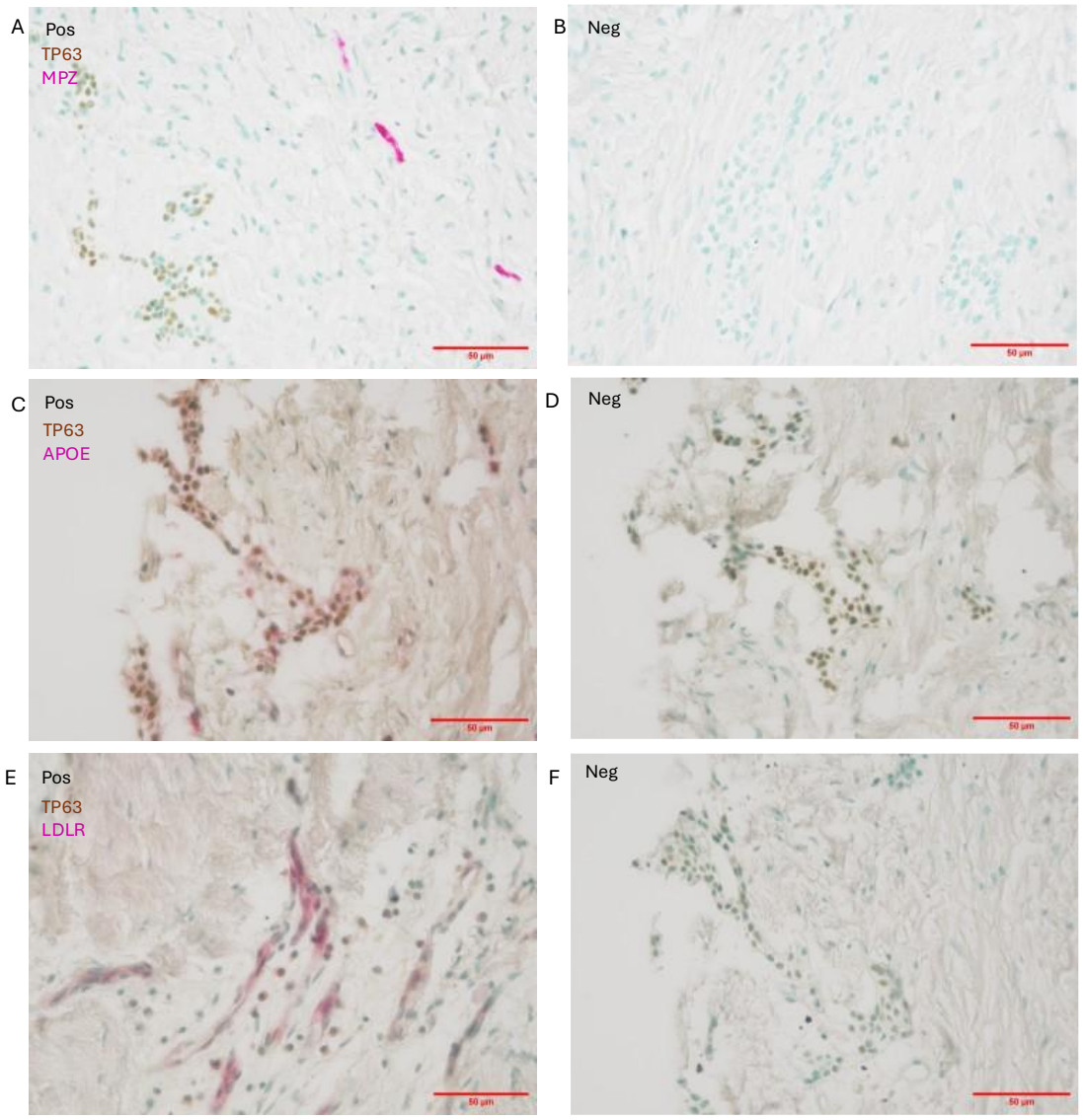

Supplementary Figure 2 – Optimization of multiplex labeling for multiple markers in DF and PDL tissues. Positive (A) and negative (B) Multiplex IHC micrographs of PDL sections stained for MPZ (pink) and TP63 (brown). Positive (C) and negative (D) Multiplex IHC micrographs of DF sections stained for APOE (pink) and TP63 (brown). Positive (E) and negative (F) Multiplex IHC micrographs of PDL sections stained for LDLR (pink) and TP63 (brown)